J Heuristics (2012) 18:169–192
DOI 10.1007/s10732-011-9166-2

GRASP and path relinking hybridizations for the point matching-based image registration problem

José Santamaría · Oscar Cordón · Sergio Damas · Rafael Martí · Ricardo J. Palma

Received: 24 June 2010 / Accepted: 25 March 2011 / Published online: 9 April 2011

Abstract In the last decade, image registration has proven to be a very active research area when tackling computer vision problems, especially in medical applications. In general, image registration methods aim to find a transformation between two images taken under different conditions. Point matching is an image registration approach based on searching for the right pairing of points between the two images, which involves a combinatorial optimization problem. From this matching, the registration transformation can be inferred by means of numerical methods.

In this paper, we tackle the medical image registration problem by means of a recent hybrid metaheuristic composed of two well-known optimization methods: GRASP and path relinking. Several designs based on this new hybrid approach have been tested. Our experimentation with real-world problems shows the combination of

J. Santamaría (✉)
Department of Computer Science, EPS de Linares, University of Jaén, C/ Alfonso X El Sabio, 28, 23700 Linares, Jaén, Spain
e-mail: jslopez@ujaen.es

O. Cordón · S. Damas
European Centre for Soft Computing, Edif. Científico-Tecnológico, C/ Gonzalo Gutiérrez Quirós, 33600 Mieres, Asturias, Spain

O. Cordón
Department of Computer Science and Artificial Intelligence, E.T.S.I. Informática y Telecomunicación, University of Granada, C. Periodista Daniel Saucedo Aranda, s.n., 18071, Granada, Spain

R. Martí
Department of Statistics and Operations Research, Facultad de Matemáticas, University of Valencia, C/ Dr. Moliner 50, 46100 Burjassot, Valencia, Spain

R.J. Palma
Department of Computer Science and Artificial Intelligence, ETSIIT, University of Granada, C/ Daniel Saucedo Aranda, 18071 Granada, Spain

GRASP and evolutionary path relinking performs well when compared to previous state-of-the-art image registration approaches adopting both the point matching and transformation parameter approaches.

Keywords Metaheuristics · GRASP · Path relinking · Scatter search · Computer vision · Medical image registration

1 Introduction

There are many applications in digital image processing that require the proper alignment of different images (Goshtasby 2005). These problems arise from rather different domains (Dasgupta and Banerjee 2005; Kim et al. 2001; Wang 2005). For example, in remote sensing, it is important to establish correspondence between the images acquired from different viewpoints in order to achieve a global cartography from partial views. In medical imaging, it is helpful to determine a correct matching between the images provided by different kinds of sensors which are able to highlight different characteristics of the human anatomy such as bones, organs, or lesions.

In the last decade, image registration (IR) has become a fundamental task in computer vision commonly used to establish correspondences (or transformations) among two or more images in order to achieve their proper alignment (Brown 1992; Zitová and Flusser 2003). There exist two different IR approaches, each one working in a different solution space: (i) to search for the optimal point matching between two images (Cordón et al. 2008; Liu 2004); and (ii) to directly search in the space of the registration transformation parameters (de Falco et al. 2008; Silva et al. 2005). While the former takes a combinatorial optimization approach, the latter does the same from a numerical (binary, integer, or real coded) optimization standpoint. In particular, point matching searches for the right pairing of points between two images, from which the registration transformation can be inferred by using numerical methods (Horn 1987). The main advantage of this IR approach is that it does not require the estimation of the suitable interval ranges of every parameter defining the transformation. Thus, the proposal of good point matching algorithms is of importance in the IR community.

In this contribution, we extend our previous work (Cordón et al. 2008) and exploit the benefits of applying the recent hybridization of the *greedy randomized adaptive search procedure* (GRASP) and the *path relinking* (PR) methodology (Resende et al. 2010) when tackling point matching-based IR problems of 3D medical images. We design our method to achieve a good trade-off between the intensification and diversification components of this hybrid approach in order to obtain high quality solutions. In line with this, it takes advantage of heuristic information extracted from the images to guide the search process. Such information corresponds to the curvature values of the object under study and has proven useful to achieve high quality solutions (Cordón et al. 2008). Furthermore, curvature information facilitates a feature-based IR approach characterized by a significant reduction of input data which are represented by the most relevant points (according to this heuristic information) of the object, thus allowing for better matching and speeding up the IR. It must be noted

that the use of problem information is in line with previous findings in different metaheuristics, such as tabu search (Glover and Laguna 1997) and contrasts with random designs typically applied in other evolutionary methods.

The performance of several designs based on GRASP and PR hybridization is compared with a previous Scatter Search-based IR method (Cordón et al. 2008) when solving six 3D medical images from realistic and real-world image datasets with different modalities: magnetic resonance images (MRIs) of human brains and computer tomography images (CTs) of human wrists, respectively.

The structure of this paper is as follows: Sect. 2 describes the point matching-based IR problem from a combinatorial optimization viewpoint. Section 3 explains the recent hybridizations of GRASP and PR algorithms that we have adapted to tackle the IR problem. Computational experiments are detailed in Sect. 4. Finally, Sect. 5 presents our concluding remarks and future works.

2 Point matching-based image registration

In this section the IR is formally described in terms of a combinatorial optimization problem. We also provide the heuristic information and the permutation-based representation scheme employed to guide the search process towards the best solutions for the point matching-based IR problem.

2.1 Problem formulation

IR can be stated as an NP-hard combinatorial optimization problem which consists of finding a mapping of points from two images: A and B, named scene and model, respectively. The objective is to determine the geometric transformation f that applied to A leading it to B (see Fig. 1).

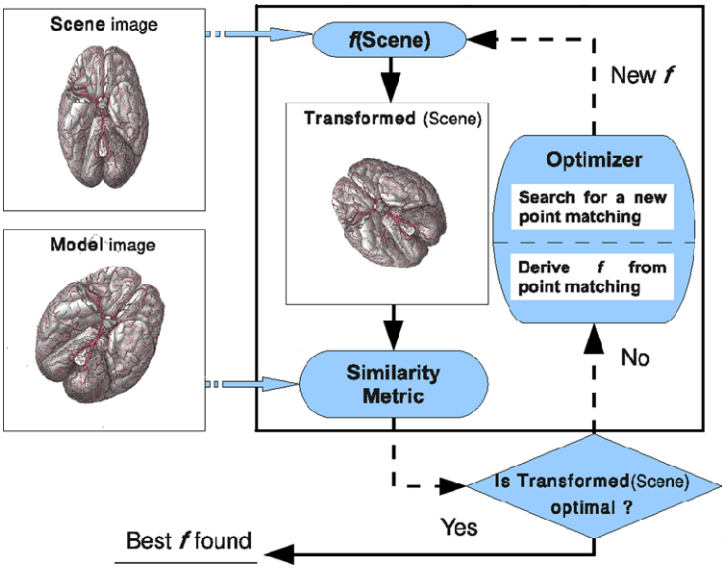

Fig. 1 The IR optimization procedure

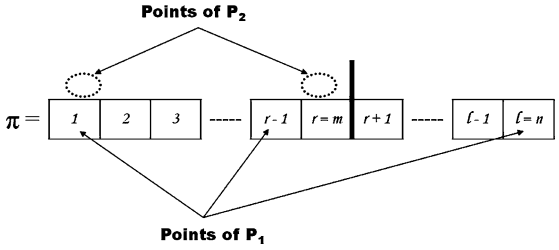

Fig. 2 Implementation details of the point matching permutation π with size n

Typically, an image is represented by a huge amount of pixels/voxels. Therefore, many IR methods apply a preprocessing step to extract the most relevant geometric primitives (points, lines, etc.) in the two images to be registered (Zitová and Flusser 2003). This is called *feature-based* IR approach and affords the advantage of speeding up the IR process and better guiding the objective function to escape from local optima (Cordón et al. 2008). In particular, we consider points defining a crest line (Monga et al. 1992) as a set of geometric primitives extracted from both images (*include several math expressions*). Crest lines are the locus of points on a surface whose longest curvature (in absolute value) is locally maximal in the associated principal direction. Thus, a crest line can be viewed as a generalization of an edge for smooth surfaces in 3D (see Sect. 2.2).

In mathematical terms, point matching can be described as a combinatorial optimization problem as follows. Given two set of points $P_1 = \{\mathbf{x}_1, \mathbf{x}_2, \ldots, \mathbf{x}_n\}$ and $P_2 = \{\mathbf{y}_1, \mathbf{y}_2, \ldots, \mathbf{y}_m\}$, the problem is to find a transformation f such that $\mathbf{y}_i = f(\mathbf{x}_{\pi(i)})$ for $i = 1, \ldots, r$ $(r = \min(n, m))$, where $\pi = (\pi_1, \pi_2, \ldots, \pi_l)$ is a permutation of size l $(l = \max(n, m))$. Without loss of generality and to simplify the notation, we consider that P_1 is the largest point set, i.e., its dimension n is greater than that one of P_2, m. Figure 2 shows a representation of the matching.

Problem solving is naturally divided into two phases. In the first one, a permutation of l elements defines the matching between the points in P_1 and P_2 in such a way that the first elements ($r = m$ in our case) of π are the P_1 points associated to each of the m P_2 points. In the second phase, from the latter point matching, the parameters defining the transformation f are computed by a numerical method (usually least squares estimation (Arun et al. 1987; Horn 1987)), the parameters defining the transformation f are computed. The goal is to find the transformation minimizing the distances between the model points and the corresponding transformed scene points. Therefore, in optimization terms, the value associated with permutation π is given by the following expression:

$$g(\pi) = \frac{\sum_{i=1}^{r} \| f_\pi(\mathbf{x}_{\pi(i)}) - \mathbf{y}_i \|^2}{r}, \tag{1}$$

i.e., Eq. 1 corresponds to the *Mean Square Error* (MSE). Therefore, the point matching problem can be simply stated as minimizing $g(\pi)$ for any permutation π of l elements and its corresponding transformation f.

2.2 Using heuristic information derived from the 3D image

This section is devoted to describe the heuristic information that can be derived from the curvature of the shapes included in the images in order to better address the optimization procedure of the IR problem.

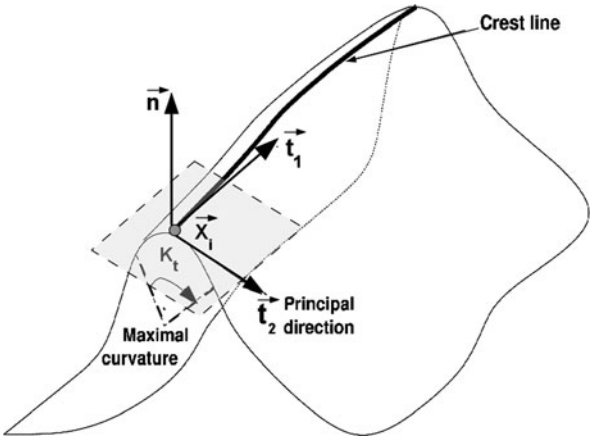

Fig. 3 Differential characteristics of surfaces

Let us first define the iso-intensity surface of a 3D image, which will be called simply the iso-surface in the rest of this paper. For any continuous function $C(x, y, z)$ of $\mathbb{R}^3$, any value I of $\mathbb{R}$ (called the iso-value) defines a continuous, not self-intersecting surface, without hole, which is called the iso-intensity surface of C (Monga et al. 1992). A non ambiguous way to define the iso-surface is to consider it as being the surface which separates the space regions where the intensity of C is greater than or equal to I from these regions whose intensity is strictly lower than I. Whether such an iso-surface corresponds or not to the boundary of the scanned object is another problem, which falls outside the scope of the current contribution. Due to their good topological properties, iso-surface techniques are the most widely used segmentation methods for 3D medical images.

Figure 3 depicts the key elements of an iso-surface. At each point $\mathbf{x}_i$ of those surfaces, there is an infinite number of curvatures but, for each direction $\mathbf{t}$ in the tangent plane at $\mathbf{x}_i$, there is only one associated curvature $k_{\mathbf{t}}$. There are two privileged directions of the surface, called the principal directions ($\mathbf{t}_1$ and $\mathbf{t}_2$), which correspond to the two extreme values of the curvature: k_1 and k_2. We limit our model to these two parameters since we have empirically found that they contain enough information to guide the search process.

In this contribution, we consider f to be a similarity transformation, thus being composed of a rotation $R = (\lambda, \langle \phi_x, \phi_y, \phi_z \rangle)$, a translation $\mathbf{t} = (t_x, t_y, t_z)$, and a uniform scaling s. Such a transformation has been extensively used to register aerial and satellite images, bony structures in medical images, and multimodal brain images (Goshtasby 2005). Once we know the expression of f_π, i.e., the $(R, \mathbf{t}, s)$ parameters defining the similarity transformation, we can estimate the registration error existing between the scene image points $\mathbf{x}_i$ and the model image points $\mathbf{y}_j$, measured by the function $g()$ as proposed in Arun et al. (1987). We estimate the registration error by simply computing the Euclidean distance from each transformed point in P_1 (using the aforementioned f_π parameters) to its corresponding matching point (considering π), as shown in Eq. 1, where $f_\pi(\mathbf{x}_{\pi_i}) = \mathbf{y} = s \cdot R(\mathbf{x}_{\pi_i}) + \mathbf{t}$.

Note that Eq. 1 only computes the geometric information of both scene and model feature points. Some authors (Luck et al. 2000; Robertson and Fisher 2002) have pro-

posed several metaheuristics to minimize the $g()$ error function. However, by considering only this objective function, search algorithms exhibit several limitations such as their inability to handle large initial misalignments between the two images, which usually makes the IR algorithm more likely to become trapped in local optima (Luck et al. 2000). To overcome these problems, we use the context information contained in the curvature. In particular, for each point x_i, we consider the two values of the first and second principal curvatures, k_1 and k_2, associated with the two principal orthogonal directions (which locally characterize the iso-surface). An interesting property of this feature is that curvature values represent an invariant source of information with respect to the similarity transformation f_π. Thus, we use a redefined function $m_{error}(\cdot)$ to evaluate the quality of the matching stored in a given solution, π, as follows:

$$m_{error}(\pi) = \Delta k_1 + \Delta k_2 \quad \text{where } \Delta k_j = \sum_{i=1}^{r} (k_j^i - k_j^{\pi_i})^2, \ j = \{1, 2\}$$

where Δk_1 and Δk_2 measure the error associated to the matching of scene and model points with different values for the first and second principal curvatures, respectively.

Hence, the proposed objective function (similarity metric) for point matching makes use of a weighted combination of the $g()$ function (MSE of the registration transformation resulting from the point matching encoded in π) and the previous criterion based on heuristic information as follows:

$$\min \ F(\pi) = w_1 \cdot g(\pi) + w_2 \cdot m_{error}(\pi) \tag{2}$$

where w_1 and w_2 are weighting coefficients defining the relative importance of each term. With such a function, we defined a more suitable similarity measure to induce a better search process in the space of solutions (Cordón and Damas 2006; Cordón et al. 2008).

3 GRASP and path relinking hybridizations

We propose different combinations of GRASP and PR for the point matching-based IR problem based on hybrid designs used in the context of the max-min diversity problem (Resende et al. 2010).

3.1 The greedy randomized adaptive search procedure

The GRASP methodology was developed in the late 1980s (Feo and Resende 1989). We refer the reader to Resende and Ribeiro (2003) for a recent survey of this metaheuristic. Each GRASP iteration consists of constructing a trial solution and then applying an improvement procedure to find a local optimum (i.e., the final solution for that iteration). The construction phase is iterative, greedy, and adaptive. It is iterative because the initial solution is built considering one element at a time. It is greedy because the addition of each element is guided by a greedy function. It is adaptive because the element chosen at any iteration in a construction is a function of

those previously chosen. The improvement phase typically consists of a local search procedure.

Our adaptation of the GRASP methodology for the point matching problem follows. The information extracted from the shape of the object (described in Sect. 2.2) can be used to establish a preference order for the assignments between the scene image points and the model image ones. Hence, a point x_i from the scene image is more likely to be assigned to those model points y_i presenting the same or similar curvature values k_1 and k_2. In order to achieve that suitable point assignment, a possible approach consists of considering a greedy heuristic. Such an approach is characterized by a strict selection order to assign the closest model point $\mathbf{y}_j$ in terms of curvature to every scene point $\mathbf{x}_i$, where $\mathbf{y}_j$ was not previously assigned to some other scene point. However, we follow a different approach by introducing randomness in both processes thus allowing each decision to be taken randomly from the points still stored in the nonempty candidate list. Specifically, the greedy randomized construction GRC starts by creating two candidate lists, CL_1 and CL_2, related to the scene and model images, respectively. At the beginning, every list consists of all the points in the image (i.e., initially $CL_1 = P_1$ and $CL_2 = P_2$). For each element $\mathbf{x}_i$ in CL_1, its Euclidean distance to CL_2 in terms of curvature values is computed as:

$$d_i = \min_{j=1,\ldots,m} \sqrt{(k_1(\mathbf{x}_i) - k_1(\mathbf{y}_j))^2 + (k_2(\mathbf{x}_i) - k_2(\mathbf{y}_j))^2}. \tag{3}$$

Thus, d_i is the minimum value of the distances from $\mathbf{x}_i$ to all the elements in CL_2. Then, the GRC phase constructs the restricted candidate list RCL_1 with a percentage α of the elements in CL_1 with the lowest d_i (high quality) values. We randomly select one element (say $\mathbf{x}_k$) from RCL_1 for the matching assignment. In order to find an appropriate point in the model to match $\mathbf{x}_k$, we construct RCL_2 with a percentage α of the elements in CL_2 whose curvature values are closer to those of $\mathbf{x}_k$, i.e., those elements presenting the lowest distance values to $\mathbf{x}_k$. Next, we randomly select a point (say $\mathbf{y}_t$) in RCL_2 and match it to $\mathbf{x}_k$. The permutation π is accordingly updated with $\pi_{(t)} = k$. Finally, we update CL_1 and CL_2 ($CL_1 = CL_1 - \{\mathbf{x}_k\}$, $CL_2 = CL_2 - \{\mathbf{y}_t\}$) and perform a new iteration. The GRC procedure finishes when $r = \min(n, m)$ points have been matched, i.e., when either CL_1 or CL_2 is empty, and the remaining $l - r$ points in the permutation π are taken randomly from the points still stored in the nonempty CL.

We also consider an alternative constructive method, GRC2, in which the greedy and the randomization rules are modified (Resende and Werneck 2004). Specifically, in the restricted candidate list RCL_1 is built considering a percentage β of randomly chosen elements in CL_1. Next, the element with the lowest d_i value is selected from RCL_1. The same approach is followed for the construction of RCL_2. Finally, we tested a parameter-free version of GRC, called the reactive-GRC (RGRC), in which the value of the parameter (α or β) is randomly determined according to an empirical distribution of probabilities (Prais and Ribeiro 2000) identified in previous construction steps of the method.

Regarding the local search (LS) phase of GRASP, we have used the strategy designed for the *Improvement Method* of the scatter search (SS)-based IR proposal designed in our previous work (Cordón et al. 2008). Therein the "best-first" LS procedure with the swapping neighbor operator is considered. In particular, swappings

are used as the primary mechanism to move from one solution to another. Moreover, two improvements were considered in order to speed up the local search procedure. A primary strategy was applied first in the neighborhood generation by only considering promising swapping moves taking as a base the curvature (heuristic) information. Then, a selective application of the local optimizer was also considered.

3.2 Path relinking

PR (Glover and Laguna 1997) is an approach proposed to integrate intensification and diversification strategies in the context of TS. This approach generates new solutions by exploring trajectories that connect high quality solutions by starting from one of these solutions, called an *initiating solution*, and generating a path in the neighborhood space that leads toward the other solutions, called *guiding solutions*. This is accomplished by selecting moves that introduce attributes contained in the guiding solutions, and incorporating them in an *intermediate solution* initially originating the initiating solution. PR was adapted in the context of GRASP as a form of intensification (Laguna and Martí 1999). The relinking in this context consists of finding a path between a solution found with GRASP and a chosen elite solution. As can be seen in different sources (see for instance http://twitter.com/graspheuristic), the hybridization of GRASP with PR has revealed itself to be a powerful metaheuristic, which is able to provide high quality solutions for different combinatorial optimization problems.

Let π^1 and π^2 be two solutions of the point matching IR problem, interpreted as the sets of n selected elements Sel_{π^1} and Sel_{π^2}, respectively ($|Sel_{\pi^1}| = |Sel_{\pi^2}| = n$). PR($\pi^1, \pi^2$) starts with the first (initiating) solution π^1, and gradually transforms it into the second (guiding) one π^2 by swapping out elements selected in π^1 with elements selected in π^2. The elements selected in both solutions π^1 and π^2, $Sel_{\pi^1\pi^2}$, remain selected in the intermediate solutions generated in the path between them. Let $Sel_{\pi^1-\pi^2}$ be the set of elements selected in π^1 and not selected in π^2. Symmetrically, let $Sel_{\pi^2-\pi^1}$ be the set of elements selected in π^2 and not selected in π^1, i.e.

$$
\begin{aligned}
Sel_{\pi^1\pi^2} &= Sel_{\pi^1} \cap Sel_{\pi^2}, \\
Sel_{\pi^1-\pi^2} &= Sel_{\pi^1} \setminus Sel_{\pi^1\pi^2}, \\
Sel_{\pi^2-\pi^1} &= Sel_{\pi^2} \setminus Sel_{\pi^1\pi^2}.
\end{aligned}
$$

Let $\pi^{ini(0)} = \pi^1$ be the initiating solution. To obtain the solution $\pi^{ini(1)}$, we unselect a single element $\pi_i^{ini(0)} \in Sel_{\pi^1-\pi^2}$ and select a single element $\pi_j^{ini(1)} \in Sel_{\pi^2-\pi^1}$ both in $\pi^{ini(0)}$, thus obtaining:

$$
Sel_{\pi^{ini(1)}} = Sel_{\pi^{ini(0)}} \setminus \{\pi_i^{ini(0)}\} \cup \{\pi_j^{ini(0)}\}.
$$

In the *greedy PR* (PR^g) algorithm, the selection of the elements $\pi_i^{ini(0)}$ and $\pi_j^{ini(0)}$ is made in a greedy fashion. To obtain $\pi^{ini(k+1)}$ from $\pi^{ini(k)}$, we evaluate all the possibilities for $\pi_i^{ini(k)} \in Sel_{\pi^{ini(k)}-\pi^2}$ to be de-selected and $\pi_j^{ini(k)} \in Sel_{\pi^1-\pi^{ini(k)}}$ to be selected, and perform the best swap. In this way, we reach π^2 from π^1 in $h = |Sel_{\pi^1-\pi^2}| = |Sel_{\pi^2-\pi^1}|$ steps, i.e. $\pi^{ini(h)} = \pi^2$. The output of the PR algorithm

is the best solution, different from π^1 and π^2, found in the path connecting both solutions (among $\pi^{ini(1)}, \pi^{ini(2)}, \ldots, \pi^{ini(h-1)}$).

Another variant of PR is based on a greedy randomized (PR^{gr}) scheme (Faria et al. 2005), in which the moves are done in a greedy randomized fashion. This procedure mimics the selection method employed in a GRASP construction. Instead of exploring all the possibilities for $\pi_i^{ini(k)} \in Sel_{\pi^{ini(k)}-\pi^2}$ to be de-selected and $\pi_j^{ini(k)} \in Sel_{\pi^2-\pi^{ini(k)}}$ to be selected to obtain $\pi^{ini(k+1)}$ from $\pi^{ini(k)}$, it can be performed a truncated exploration of a certain percentage of the whole neighborhood in order to speed up the run time. Thus, the candidate set C contains all these swaps, i.e.

$$C^k_{\pi^1\pi^2} = \{(\pi_i^{ini(k)}, \pi_j^{ini(k)}) \mid i \in Sel_{\pi^{ini(k)}-\pi^2}, j \in Sel_{\pi^2-\pi^{ini(k)}}\}.$$

Let $z(i, j)$ be the value of the move associated with de-select $\pi_i^{ini(k)}$ and select $\pi_j^{ini(k)}$ in the current solution $\pi^{ini(k)}$ to obtain $\pi^{ini(k+1)}$. Then,

$$z(i, j) = F(\pi^{ini(k+1)}) - F(\pi^{ini(k)}).$$

In step k of the path from π^1 to π^2, the restricted candidate list $RCL^k_{\pi^1\pi^2}$ of good candidates for swapping is

$$RCL^k_{\pi^1\pi^2} = \{(\pi_i^{ini(k)}, \pi_j^{ini(k)}) \in C^k_{\pi^1\pi^2} \mid z(i, j) \geq \delta z^*\},$$

where z^* is the minimum of $z(i, j)$ in $C^k_{\pi^1\pi^2}$ and δ ($0 \leq \delta \leq 1$) is a search parameter. A pair $(\pi_i^{ini(k)}, \pi_j^{ini(k)}) \in RCL^k_{\pi^1\pi^2}$ is randomly selected and the associated swap is performed.

Furthermore, PR can be performed bi-directionally by exploring the two possible paths connecting two given solutions. The best solution found is accordingly returned. Regarding the computation time, improved performance can be achieved by considering a pruning scheme for the neighborhood exploration of PR based on the heuristic information extracted from the image. This strategy, also called truncated path relinking, is inspired by the observation that as the PR nears the guiding solution, there are fewer allowed moves to explore and the search tends to be less effective. Hence, it tends to find good solutions near the initiating one since it can explore the space more effectively around the latter. If this happens, then the effort made by path relinking near the guiding solution is fruitless. Therefore, we can prune (truncate) the path when a percentage of solutions has been explored, applying an early stopping criterion to save computational effort.

3.3 Static GRASP with PR

In Stc-G&PR, we propose a static hybridization in which we first apply GRASP to construct the elite set (ES) (see steps 1 to 14 in Fig. 4) and then, as a second step, we apply PR to generate solutions between all the pairs of solutions in ES (see steps 15 to 24 in Fig. 4). As shown in Fig. 4, we always keep the best solution in ES (π^1) during performance of the GRASP and the LS phases. Note the use of a distance

Begin Stc-G&PR

1 *GlobalIter* ← number of global iterations;
2 Apply GRASP (construction and local search) for $b = |ES|$ iterations to populate $ES \leftarrow \{\pi^1, \pi^2, \ldots, \pi^b\}$;
3 *NumIter* ← $b + 1$;
4 **While** *NumIter* ≤ *GlobalIter* **Do**
5 $\pi \leftarrow$ GRASP construction phase;
6 $\pi' \leftarrow$ GRASP LS starting at π;
7 $\pi^k \leftarrow$ closest solution to π' in *ES* with $F(\pi') < F(\pi^k)$;
8 $ES' \leftarrow \{ES \setminus \pi^k\} \cup \pi'$;
9 **If** $F(\pi') < F(\pi^1)$ **Or** $(F(\pi') < F(\pi^b)$ **And** Div$(ES') \geq$ Div$(ES))$ **Then**
10 Add π' to *ES* and remove π^k;
11 Sort *ES* from best π^1 to worst π^b;
12 **End-If**;
13 *NumIter* ← *NumIter* + 1;
14 **End-While**;
15 $\pi^{best} \leftarrow \pi^1$;
16 **For** $i = 1, \ldots, b-1$ **Do**
17 **For** $j = i+1, \ldots, b$ **Do**
18 Apply PR(π^i, π^j) and PR(π^j, π^i) and let π' be the best solution found;
19 $\pi'' \leftarrow$ GRASP LS starting at π';
20 **If** $(F(\pi'') < F(\pi^{best}))$ **Then**
21 $\pi^{best} \leftarrow \pi''$;
22 **End-If**;
23 **End-For**;
24 **End-For**;
25 **Return** π^{best};

End-Stc-G&PR

Fig. 4 Pseudo-code of the Stc-G&PR algorithm

considered to measure how diverse one solution is with respect to a set of solutions, which is ES in this case. Specifically, for the point matching we consider the distance between two permutations π^a and π^b as the number of times $\pi^a_{(i)}$ differs from $\pi^b_{(i)}$ for $i = 1, \ldots, r$. Then, the candidate solution π' is considered for inclusion in ES if its quality surpasses (according to $F()$ value) either the current best in ES (π^1), or the current worst in ES (π^b) and it also increases the diversity of ES (Div(*ES*)) by means of replacing $\pi^k \in ES$ with π' ($ES \leftarrow \{ES \setminus \pi^k\} \cup \pi'$). In the second step of the algorithm, for each pair of solutions $\{\pi^a, \pi^b\} \in ES$, we apply PR in a bidirectional manner, i.e. PR(π^a, π^b) and PR(π^b, π^a). Next, the best solution generated in both paths is subjected to the LS method (described in Sect. 3.1). Stc-G&PR stops once PR is applied to all the pairs in ES and the best overall solution x^{best} is returned as the output.

Unlike in Resende et al. (2010), in our specific implementation of point matching the *dth* parameter (which is a distance threshold value that reflects the term "sufficiently different" and it should be empirically adjusted) has been properly removed from Stc-G&PR (see line 9 in Fig. 4) as well as from the subsequent hybrids.

Begin Dyn-G&PR

1 *GlobalIter* ← number of global iterations;
2 Apply GRASP (construction and local search) for $b = |ES|$ iterations to populate $ES \leftarrow \{\pi^1, \pi^2, \ldots, \pi^b\}$;
3 *NumIter* ← $b + 1$;
4 **While** *NumIter* ≤ *GlobalIter* **Do**
5 $\pi \leftarrow$ GRASP construction phase;
6 $\pi' \leftarrow$ GRASP LS starting at π;
7 Randomly select π^j from *ES*;
8 Apply PR(π', π^j) and PR(π^j, π') and let π'' be the best solution found;
9 $\pi''' \leftarrow$ GRASP LS starting at π'';
10 $\pi^k \leftarrow$ closest solution to π''' in *ES* with $F(\pi''') < F(\pi^k)$;
11 $ES' \leftarrow \{ES \setminus \pi^k\} \cup \pi'''$;
12 **If** $F(\pi''') < F(\pi^1)$ **Or** $(F(\pi''') < F(\pi^b)$ **And** Div(ES') ≥ Div(*ES*)) **Then**
13 Add π''' to *ES* and remove π^k;
14 Sort *ES* from best π^1 to worst π^b;
15 **End-If**;
16 *NumIter* ← *NumIter* + 1;
17 **End-While**;
18 $\pi^{best} \leftarrow \pi^1$;
19 **Return** π^{best};

End-Dyn-G&PR

Fig. 5 Pseudo-code of the Dyn-G&PR algorithm

3.4 Dynamic GRASP with PR

Another alternative of hybrid implementation using GRASP and PR algorithms consists of a dynamic update of ES, we called it Dyn-G&PR. In this design, each solution π' generated with GRASP is directly subjected to the PR algorithm, which is applied between π' and a solution π^j, randomly selected from ES. As in Stc-G&PR, the LS method is applied to the output of PR. In this case, the resulting solution is directly tested for inclusion in ES. If successful, it can be used as a guiding solution in later applications of PR. Figure 5 shows pseudo-code for this dynamic variant. The method stops after Globaliter number of iterations.

3.5 Evolutionary GRASP with PR

Evolutionary GRASP with PR (Andrade and Resende 2007), Evo-G&PR, starts in the same way as dynamic GRASP with PR, Dyn-G&PR. This can be clearly seen in the first steps (1–16) of Fig. 6. Specifically, Dyn-G&PR is applied for *GlobalIter* number of iterations, in which the construction and the improvement phase of GRASP as well as the PR method are executed. At this point, a post-processing phase is applied for improved outcomes. Specifically, we apply PR to each pair of solutions in ES (steps 17 to 30 in Fig. 6). The solutions obtained with the latter application of PR are considered candidates to enter ES, and PR is again applied to them as long as a new solution is able to enter ES. Hence, solutions in ES evolve and the method stops when no new solutions update ES.

Begin Evo-G&PR

1 *GlobalIter* ← number of global iterations;
2 Apply GRASP (construction and local search) for $b = |ES|$ iterations to populate $ES \leftarrow \{\pi^1, \pi^2, \ldots, \pi^b\}$;
3 **For** $iter = 1, \ldots,$ *GlobalIter* **Do**
4 **For** $i = 1, \ldots,$ *LocalIter* **Do**
5 $\pi \leftarrow$ GRASP construction phase;
6 $\pi' \leftarrow$ GRASP LS starting at π;
7 Randomly select π^j from *ES*;
8 Apply PR(π', π^j) and PR(π^j, π') and let π'' be the best solution found;
9 $\pi''' \leftarrow$ GRASP LS starting at π'';
10 $\pi^k \leftarrow$ closest solution to π''' in *ES* with $F(\pi''') < F(\pi^k)$;
11 $ES' \leftarrow \{ES \setminus \pi^k\} \cup \pi'''$;
12 **If** $F(\pi''') < F(\pi^1)$ **Or** ($F(\pi''') < F(\pi^b)$ **And** Div(ES') ≥ Div(*ES*)) **Then**
13 Add π''' to *ES* and remove π^k;
14 Sort *ES* from best π^1 to worst π^b;
15 **End-If**;
16 **End-For**;
17 *NewSol* ← 1;
18 **While** *NewSol* **Do**
19 *NewSol* ← 0;
20 Apply PR(π, π') and PR(π', π) for every pair (π, π') in *ES* not combined before. Let π'' be the best solution found;
21 $\pi''' \leftarrow$ GRASP LS starting at π'';
22 $\pi^k \leftarrow$ closest solution to π''' in *ES* with $F(\pi''') < F(\pi^k)$;
23 $ES' \leftarrow \{ES \setminus \pi^k\} \cup \pi'''$;
24 **If** $F(\pi''') < F(\pi^1)$ **Or** ($F(\pi''') < F(\pi^b)$ **And** Div(ES') ≥ Div(*ES*)) **Then**
25 Add π''' to *ES* and remove π^k;
26 Sort *ES* from best π^1 to worst π^b;
27 *NewSol* ← 1;
28 $\pi^{best} \leftarrow \pi^1$;
29 **End-If**;
30 **End-While**;
31 **End-For**;
32 **Return** π^{best};

End-Evo-G&PR

Fig. 6 Pseudo-code of the Evo-G&PR algorithm

Note that this design can be considered similar in general terms to other evolutionary methods, such as scatter search, in which solutions in the reference set (the elite set where the best solutions are stored) evolve by means of combinations. However, in Evo-G&PR instead of combinations we apply PR, which is somewhat a generalization of the classical combination methods. Moreover, we apply PR from the very beginning of the execution, making the search aggressive (i.e. obtaining high-quality solutions in early stages of the method).

4 Computational experiments

This section describes the computational experiments we performed to compare our proposed procedures to state-of-the-art methods for solving medical IR problems.

Our GRASP with PR implementations follows the framework described in the previous section. We first set the key search parameters of our methods and then study their effectiveness and robustness, including comparisons with a recent scatter search algorithm (Cordón et al. 2008) and three state-of-the-art methods. All the methods have been implemented in C/C++ programming and tested in the same architecture using a 2.26 GHz Intel® Core™2 Duo P8400 and a MS® Windows operating system.

We consider six medical images from two different image datasets to test our methods. The first dataset is composed of four different magnetic resonance images (MRIs). These images have been obtained from the *BrainWeb* database at McGill University (Kwan et al. 1999). The purpose of this repository is to provide researchers with ground truth data for image analysis techniques and algorithms. *BrainWeb* has been widely used by the IR research community (see, for example Wachowiak et al. 2004). One of the most challenging IR problems concerns registering *different pairs of images of the same object*. Therefore, we tackle a more realistic problem in medical IR, namely *intra-subject registration*, than the one considered in Cordón and Damas (2006). The other two images considered belong to a second dataset of a real-world medical case study kindly provided by the Rhode Island Hospital (Marai et al. 2006). Both are computerized tomography (CT) images of two different human wrists. In this case, we want to highlight the complexity of the problem to be tackled due to its particular anatomical structure. After pre-processing, the six images (I_1 to I_6) present 583, 393, 348, 284, 575, and 412 crest line points respectively.

The first column of Figs. 7 and 8 show the original MRIs and CTs, respectively. The second column of those figures corresponds to the isosurfaces segmenting the original images to extract the regions of interest in each image, i.e. the brain and the wrist. The third column shows the crest line points extracted from each 3D medical image.

In order to evaluate the performance of the IR methods tested, we considered four similarity transformations (see Sect. 2.2) T_i (see Table 1), each one describing a different level of misalignment between a pair of images (Cordón and Damas 2006).

4.1 Fine tuning and alternative designs

In our first preliminary experiment we compare the performance of the constructive algorithms: GRC and GRC2 with $\alpha, \beta \in \{0.75, 0.9, 0.95\}$, and their reactive versions, reactive-GRC (RGRC) and reactive-GRC2 (RGRC2). To do so, sixteen IR problem instances (see Table 2) have been designed from the combination of the considered image datasets of MRIs of human brains and the four similarity transformations (see Fig. 7 and Table 1, respectively). Each of the latter four variants of GRASP has been run once considering a maximum number of one hundred iterations of the construction and the LS phases. We keep the same parameter settings for the LS method as in Cordón et al. (2008).

Both the first (*#better*) and the second (*Divergence*) rows in Table 3 show the average value of: (i) the percentage of times in which a given GRC variant achieved a solution as good as the best found so far in each of the one hundred iterations; and (ii) the divergence of a given GRC variant to the best GRC variant according to MSE

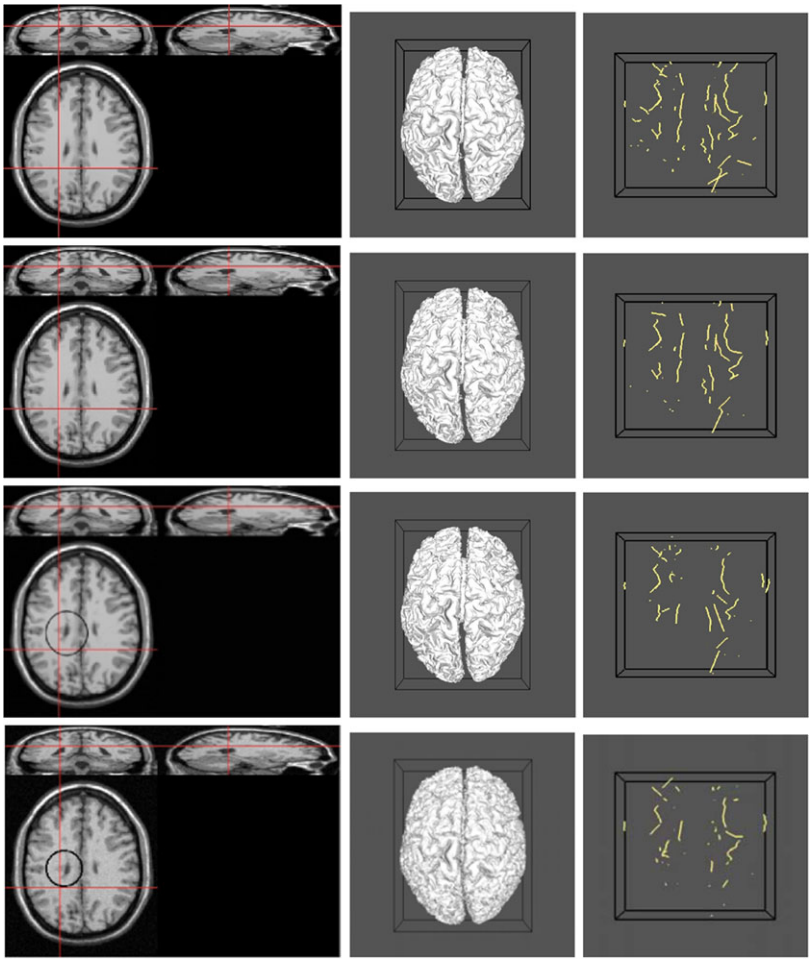

Fig. 7 *From left to right*, and *top to bottom*: original MRI images, their respective isosurfaces, and their crest lines points. Note that the second and third MRIs include 1% of Gaussian noise while the fourth one has a 5%. I_3 and I_4 (*last two rows*) also considers a multiple sclerosis lesion (see *circle*)

values. From these results, we remark that the GRC variant considering $\alpha = 0.9$ is the best alternative to construct solutions for GRASP. Thus, this will be our choice for the subsequent experiments.

In our second preliminary experiment we study the best configuration of PR when hybridized with GRASP. Specifically, we consider the Stc-G&PR approach (described in Sect. 3.3) and compare the following twelve PR designs described in Sect. 3.2:

– $PR_1 : PR^g$ & uni-directional[1]

[1] An unidirectional scheme considers the construction of one solution following the route that connects the initial with the guiding solution. On the other hand, a bi-directional scheme performs the construction

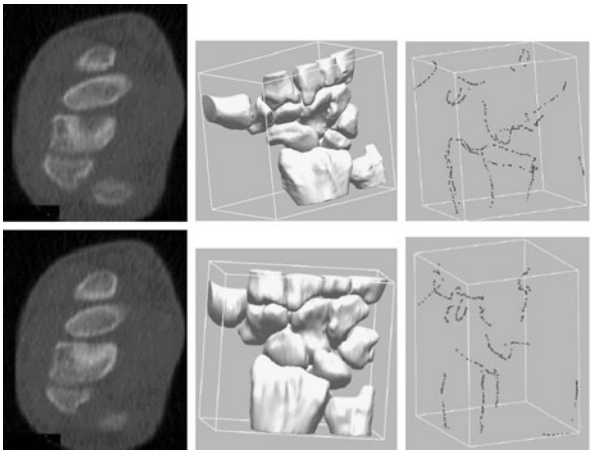

Fig. 8 *From left to right*: original CT images, their respective isosurfaces, and their crest lines points. The *first* and *second rows* refer to I_5 and I_6, respectively

Table 1 Similarity transformations considered

	T_1	T_2	T_3	T_4
λ	115.0	168.0	235.0	276.9
ϕ_x	−0.863868	0.676716	−0.303046	0.872872
ϕ_y	0.259161	−0.290021	−0.808122	0.436436
ϕ_z	0.431934	0.676716	0.505076	−0.218218
t_x	−26.0	6.0	16.0	12.0
t_y	15.5	5.5	−5.5	5.5
t_z	−4.6	−4.6	−4.6	−24.6
s	1.0	0.8	1.0	1.2

Table 2 The sixteen IR problem instances designed considering the realistic case of study of human brains, with $T_i = T_1, \ldots, T_4$ (see Table 1)

IR problem	Scene image		Model image	
	Lesion	Noise	Lesion	Noise
I_1 vs. $T_i(I_2)$	No	No	No	1%
I_1 vs. $T_i(I_3)$	No	No	Yes	1%
I_1 vs. $T_i(I_4)$	No	No	Yes	5%
I_2 vs. $T_i(I_4)$	No	1%	Yes	5%

– $PR_2 : PR^g$ & bi-directional
– $PR_3 : PR_1$ & pruning the 30% of the path
– $PR_4 : PR_1$ & pruning the 50% of the path
– $PR_5 : PR_2$ & pruning the 30% of the path
– $PR_6 : PR_2$ & pruning the 50% of the path
– $PR_7 : PR^{gr}$ & uni-directional

of two solutions considering the two possible routes (i.e. from the initial to the guiding solution, and the reverse route) and the best one is accordingly selected.

Table 3 Results obtained by each of the eight considered variants of GRC

	$GRC_{0.75}$	$GRC_{0.9}$	$GRC_{0.95}$	$RGRC$	$GRC2_{0.75}$	$GRC2_{0.9}$	$GRC2_{0.95}$	$RGRC2$
#better (%)	3	**11**	8	8	2	0	0	9
Divergence	7.63	**1.81**	4.93	6.48	33.88	50.05	67.87	4.90

Table 4 The four IR problem instances designed considering the realistic case of study of human brains, with $T_i = T_1, \ldots, T_4$ (see Table 1)

IR problem	Scene image		Model image	
	Lesion	Noise	Lesion	Noise
I_1 vs. $T_1(I_2)$	No	No	No	1%
I_1 vs. $T_2(I_3)$	No	No	Yes	1%
I_1 vs. $T_3(I_4)$	No	No	Yes	5%
I_2 vs. $T_4(I_4)$	No	1%	Yes	5%

Table 5 MSE results obtained by each of the twelve variants of PR when using or not a pruning scheme

	Without pruning				With pruning			
	min	max	μ	σ	min	max	μ	σ
PR_1	51.00	140.55	84.43	34.04	53.18	170.58	95.03	46.04
PR_2	52.13	129.89	82.32	32.59	47.51	149.08	87.69	40.35
PR_3	51.44	172.71	89.79	49.37	47.44	188.07	96.58	54.82
PR_4	48.10	140.84	92.08	43.24	45.72	249.35	117.29	81.99
PR_5	46.04	133.51	80.46	36.14	**43.11**	153.79	96.18	45.58
PR_6	53.82	164.15	89.88	44.52	55.58	151.83	85.21	39.30
PR_7	52.74	160.49	89.82	43.18	43.74	150.94	87.68	42.87
PR_8	52.93	154.38	89.42	38.80	52.71	127.10	**82.39**	27.35
PR_9	**44.31**	168.62	89.27	49.29	54.60	139.12	91.08	35.86
PR_{10}	45.49	141.22	**78.14**	38.56	45.08	148.52	93.92	43.40
PR_{11}	47.34	153.65	86.05	43.02	57.52	170.12	96.81	45.36
PR_{12}	47.29	136.64	82.12	35.54	45.55	150.30	83.15	41.19

– $PR_8 : PR^{gr}$ & bi-directional
– $PR_9 : PR_7$ & pruning the 30% of the path
– $PR_{10} : PR_7$ & pruning the 50% of the path
– $PR_{11} : PR_8$ & pruning the 30% of the path
– $PR_{12} : PR_8$ & pruning the 50% of the path

We study four different IR problem instances (see Table 4) designed from the combination of the MRIs of human brains and the four similarity transformations (see Fig. 7 and Table 1, respectively). The size of ES was set to 6. Each of the latter twelve variants of Stc-G&PR has been run once with a maximum CPU time of 600 seconds.

Table 5 depicts the statistical results achieved by each of the variants of PR when tackling every of the four IR problem instances (e.g., I_1 vs. $T_1(I_2)$, I_1 vs. $T_2(I_2)$, I_1

vs. $T_3(I_2)$, and I_1 vs. $T_4(I_2)$) of their corresponding scenarios (I_1 vs. $T_i(I_2)$). According to mean values, we can see how the PR variants provide better performance when the pruning scheme is not considered. The latter behavior is corroborated by the higher values of standard deviation obtained when such a scheme is used. Regarding the minimum and the mean MSE values, it is proven that PR_{10} (which makes use of a greedy randomized scheme for movement selection of PR and follows a pruning scheme of 50% of the unidirectional path) is the best choice among all the variants. Thus, we will consider this variant for the subsequent experiments.

4.2 Final designs and previous methods

In our next experiment we analyze the effectiveness of each of the three hybrids based on GRASP and PR, Stc-G&PR, Dyn-G&PR, and Evo-G&PR. Moreover, we also include a pure GRASP (using GRC and $\alpha = 0.9$) and the previous method based on scatter search (Cordón et al. 2008). Each of the five IR methods is run once considering a maximum CPU time of 600 seconds on each problem instance (described in Table 2).

Table 6 is split into four subtables considering every IR problem scenario (I_1 vs. $T_i(I_2)$, I_1 vs. $T_i(I_3)$, I_1 vs. $T_i(I_4)$, and I_2 vs. $T_i(I_4)$). The best MSE value is shown in underlined bold font for each of the sixteen IR problem instances. We remark the poor performance obtained by the pure GRASP which only achieves the best MSE value in one of the sixteen instances. On the contrary, the hybrid GRASP with PR variants proposed for point matching-based IR achieved competitive results when compared to the state-of-the-art algorithm based on SS, which obtained the best MSE value in six of the sixteen instances. The remaining best MSE values (nine) were shared out amongst the three proposed hybrids. Specifically, Table 7 shows how both the SS and the Evo-G&PR methods achieved the best average effectiveness when tackling the point matching IR problem. Hence, we can see how Evo-G&PR obtains high quality solutions for the IR problem, as it has previously done in other challenging problems (Resende and Werneck 2004; Resende et al. 2010).

To complement this analysis, we again consider our three GRASP with PR hybridization-based IR proposals, a pure GRASP and the previous SS, but now we enrich the IR problem instances by including the real-world case study based on the image dataset of human wrists of CTs. Specifically, we considered the five IR problem instances shown in Table 8.

Moreover, we included three different IR state-of-the-art methods in order to highlight the computational results of this final experiment. Specifically, we considered the following parameter setting for each of them:

- The ICP+SA algorithm is run for one complete iteration with a maximum of 40 iterations for the wrapped improved version of the ICP algorithm (I-ICP) (Liu 2004). The annealing process has 20 iterations and 50 trial movements around each annealing iteration, with an initial temperature value estimated with $T_0 = [\mu/-\ln(\phi)]C(S_0)$, where $C(S_0)$ is the cost of the given solution generated by the previous run of I-ICP, and both the μ and the ϕ factors take value 0.3.
- In the dynamic GA (Dyn-GA) (Chow et al. 2004), the size of the initial population has been established at 100 individuals and the remainder of the specific parameters have retained their original values.

Table 6 MSE values obtained by the three hybrids (Stc-G&PR, Dyn-G& PR, and Evo-G&PR), the pure GRASP, and the state-of-the-art IR algorithm based on SS for the IR problem instances in Table 4

T_1	Stc-G&PR	Dyn-G&PR	Evo-G&PR	GRASP	SS	T_2	Stc-G&PR	Dyn-G&PR	Evo-G&PR	GRASP	SS
	39.06	45.39	43.86	46.22	40.45		**27.64**	42.63	42.66	31.32	40.43
I_1 vs. $T_i(I_2)$											
T_3	Stc-G&PR	Dyn-G&PR	Evo-G&PR	GRASP	SS	T_4	Stc-G&PR	Dyn-G&PR	Evo-G&PR	GRASP	SS
	57.14	73.16	73.48	**48.43**	73.07		**47.53**	51.03	50.49	67.62	48.18
T_1	Stc-G&PR	Dyn-G&PR	Evo-G&PR	GRASP	SS	T_2	Stc-G&PR	Dyn-G&PR	Evo-G&PR	GRASP	SS
	77.34	**77.30**	79.44	115.76	86.33		53.34	**44.25**	46.30	55.49	44.83
I_1 vs. $T_i(I_3)$											
T_3	Stc-G&PR	Dyn-G&PR	Evo-G&PR	GRASP	SS	T_4	Stc-G&PR	Dyn-G&PR	Evo-G&PR	GRASP	SS
	93.11	76.87	**64.70**	116.26	66.42		125.32	**107.90**	109.92	170.59	112.36
T_1	Stc-G&PR	Dyn-G&PR	Evo-G&PR	GRASP	SS	T_2	Stc-G&PR	Dyn-G&PR	Evo-G&PR	GRASP	SS
	65.26	88.63	91.47	118.74	79.59		60.85	36.35	39.18	84.03	**36.32**
I_1 vs. $T_i(I_4)$											
T_3	Stc-G&PR	Dyn-G&PR	Evo-G&PR	GRASP	SS	T_4	Stc-G&PR	Dyn-G&PR	Evo-G&PR	GRASP	SS
	85.96	63.98	**62.11**	111.09	64.90		104.41	83.80	82.19	139.46	**81.02**
T_1	Stc-G&PR	Dyn-G&PR	Evo-G&PR	GRASP	SS	T_2	Stc-G&PR	Dyn-G&PR	Evo-G&PR	GRASP	SS
	107.44	88.59	87.91	113.93	**83.41**		54.07	44.58	41.44	72.33	**38.83**
I_2 vs. $T_i(I_4)$											
T_3	Stc-G&PR	Dyn-G&PR	Evo-G&PR	GRASP	SS	T_4	Stc-G&PR	Dyn-G&PR	Evo-G&PR	GRASP	SS
	105.50	88.40	87.82	131.17	**86.48**		117.86	92.13	92.69	179.37	**78.70**

Table 7 Overall effectiveness of each of the IR methods averaging their corresponding sixteen MSE values from Table 6

	Stc-G&PR	Dyn-G&PR	Evo-G&PR	GRASP	SS
μ	76.37	69.06	68.48	100.11	**66.33**

Table 8 The five IR problem instances designed considering realistic and real-world cases of study of human brains and human wrists, respectively

IR problem	Scene image		Model image	
	Lesion	Noise	Lesion	Noise
I_1 vs. $T_1(I_2)$	No	No	No	1%
I_1 vs. $T_2(I_3)$	No	No	Yes	1%
I_1 vs. $T_3(I_4)$	No	No	Yes	5%
I_2 vs. $T_4(I_4)$	No	1%	Yes	5%
I_6 vs. $T_1(I_5)$	–	–	–	–

– The iterated local search (ILS) IR method (Cordón and Damas 2006) is based on the same optimization approach as the IR algorithms tested in this work using permutations for representation of the point matching IR approach (see Sect. 2.1). The perturbation rate and the remainder of control parameters have been maintained from the original design.

Notice how ILS and Dyn-GA adopt approaches employing point matching and transformation parameters, respectively, while ICP+SA makes use of a cooperative design of both approaches. Thus, we considered using the following objective function proposed in Cordón et al. (2006) for both the Dyn-GA and the annealing stage of ICP+SA:

$$F(f, I_s, I_m) = \omega_1 \cdot \left(\frac{1}{1 + \sum_{i=1}^{N} \|(sR(\mathbf{p}_i) + \mathbf{t}) - \mathbf{p}'_j\|^2} \right) + \omega_2 \cdot \left(\frac{1}{1 + |\rho_c^s - \rho^m|} \right) \tag{4}$$

where I_s and I_m are the scene and model images; f is the transformation encoded in the evaluated solution; $\mathbf{p}_i$ is the i^{th} 3D point from the scene and $\mathbf{p}'_j$ is its corresponding closest point in the model obtained with the GCP data structure (Yamany et al. 1999); ω_1 and ω_2 ($\omega_1 + \omega_2 = 1$) weight the importance of each function term; ρ_c^s is the radius of the sphere wrapping up the scene image transformed with the current f; and ρ^m is the radius of the sphere wrapping up the model image. As the first term of F reveals, the modeled error corresponds to the MSE. Note that F maximizes up to 1.0 for an infrequent perfect fit.

Finally, each of the eight IR methods has been run[2] ten times and considering a maximum CPU time of 600 seconds, except ICP+SA which is iteration-based.

From Table 9, we notice how the Evo-G&PR-based IR method achieves a competitive performance compared to the state-of-the-art IR algorithm based on SS. Specif-

[2]Each run uses a different seed for the pseudo-random number generator in order to avoid the bias of randomness.

Table 9 Statistical results computed from ten runs performed on each of the eight IR problems considered. The minimum (m), maximum (M), mean (μ), and standard deviation (σ) values of MSE. The best results according to mean and standard deviation values are highlighted. The last row refers to the averaged performance considering the eight IR problems at once

		Stc-G&PR	Dyn-G&PR	Evo-G&PR	GRASP	SS	ILS	ICP + SA	Dyn-GA
I_1 vs. $T_1(I_2)$	min	46.59	40.82	41.79	44.09	**39.70**	125.37	85.76	138.82
	max	59.14	49.38	47.26	58.27	45.53	291.89	88.17	300.96
	μ	50.48	44.22	44.43	50.39	**42.85**	216.84	87.93	206.86
	σ	4.23	2.42	1.86	4.84	1.88	59.33	0.72	47.55
I_1 vs. $T_2(I_3)$	min	42.37	39.93	**39.17**	44.16	40.77	40.50	237.23	87.60
	max	64.85	49.58	45.05	91.74	49.71	285.17	296.84	211.83
	μ	50.20	43.34	**43.22**	60.44	44.62	164.15	261.65	152.48
	σ	6.45	2.77	1.76	13.59	2.23	102.34	18.07	39.17
I_1 vs. $T_3(I_4)$	min	81.37	58.66	57.41	83.25	**57.37**	95.56	61.23	55.94
	max	100.57	64.51	62.73	141.04	64.90	466.31	95.59	367.47
	μ	88.94	61.04	**60.88**	108.60	61.18	276.18	64.67	171.29
	σ	6.15	1.76	1.57	18.62	1.88	122.45	10.31	79.28
I_2 vs. $T_4(I_4)$	min	120.22	85.32	81.00	136.10	**78.70**	151.13	961.65	170.04
	max	168.34	105.52	91.89	228.06	95.02	645.93	1532.82	307.95
	μ	143.76	94.14	88.51	156.38	**87.80**	428.10	1247.23	253.50
	σ	14.74	6.12	3.59	26.49	5.19	170.17	208.71	41.97
I_6 vs. $T_1(I_5)$	min	1.87	1.74	1.68	2.26	**1.63**	1.48	2.52	3.68
	max	3.47	1.89	1.95	3.57	3.99	3.44	3.60	12.24
	μ	2.70	1.81	**1.80**	2.88	2.19	2.58	3.25	5.69
	σ	0.52	0.04	0.10	0.44	0.83	0.64	0.26	2.37
	μ	67.22	48.91	47.77	75.74	**47.73**	217.57	332.94	157.96

ically, the former algorithm achieves the best mean results for three of the five IR problem instances. Moreover, it obtains the lowest standard deviation values in all the cases. Therefore, Evo-G&PR-based provides a good trade-off between search space diversification and intensification, thus showing more robust behavior than the SS-based IR method, the pure GRASP, and its counterpart hybrids: Stc-G&PR and Dyn-G&PR. Regarding accuracy of the approaches (i.e. minimum value of MSE), both SS and Evo-G&PR IR methods behave in very similarly, obtaining accurate results when tackling IR problem instances involving MRIs. The last row in Table 9 shows the average/overall performance (regarding the mean value of MSE) of each of the IR methods compared to tackle both the realistic and the real-world case studies. The latter results reveal that, both Evo-G&PR and SS methods performed best according to the overall robustness of the methods tackling the point matching-based IR problem. This behavior is similar to that shown by both methods in terms of effectiveness.

Regarding the results obtained by the state-of-the-art IR algorithms, their performance is noticeably lower than the best ones analyzed in this work (Stc-G&PR, Dyn-G&PR, Evo-G& PR, GRASP, and SS). Among the former three algorithms, only ICP+SA and ILS show competitive results in the third and fifth problem instances, respectively, but far from the best results achieved by the two best IR proposals based on SS and Evo-G&PR. The poor performance of Dyn-GA is related to the restart strategy designed by the authors to provide an IR method for working on reduced search spaces in order to achieve precise alignment results.

Figure 9 represents these results graphically for the five best IR methods globally (according to the numerical results in Table 9): pure GRASP, Stc-G&PR, Dyn-G&PR, Evo-G&PR, and SS. The first column in Fig. 9 corresponds to the initial configurations of the four different IR problem instances of MRIs. The next columns show the best IR results obtained by the compared methods: pure GRASP, Stc-G&PR, Dyn-G&PR, Evo-G&PR, and SS, respectively. Notice that the initial configurations considered correspond to important misalignment of the images. Hence, the IR problem instances tackled are highly complex. Even dealing with such complex scenarios, both Evo-G&PR and SS methods achieve outstanding best solutions. That is visually shown by the almost perfect overlapping of the colors of the objects in the fifth and sixth columns of Fig. 9. The visual results corresponding to the IR of CT images, i.e. I_6 vs. $T_1(I_5)$ (see Fig. 10) show the high complexity of this real-world case study, mainly caused by the nature of the anatomical structure of the human wrist. Again, it can be observed how the two said methods provide the best results.

5 Conclusions and future works

We have presented a contribution to undertake a challenging real-world computer vision problem by means of recent hybridizations of GRASP and PR algorithms. Specifically, in this work we have proposed several advanced hybridization designs to tackle the point matching-based IR problem based on a static, a dynamic, and an evolutionary approach.

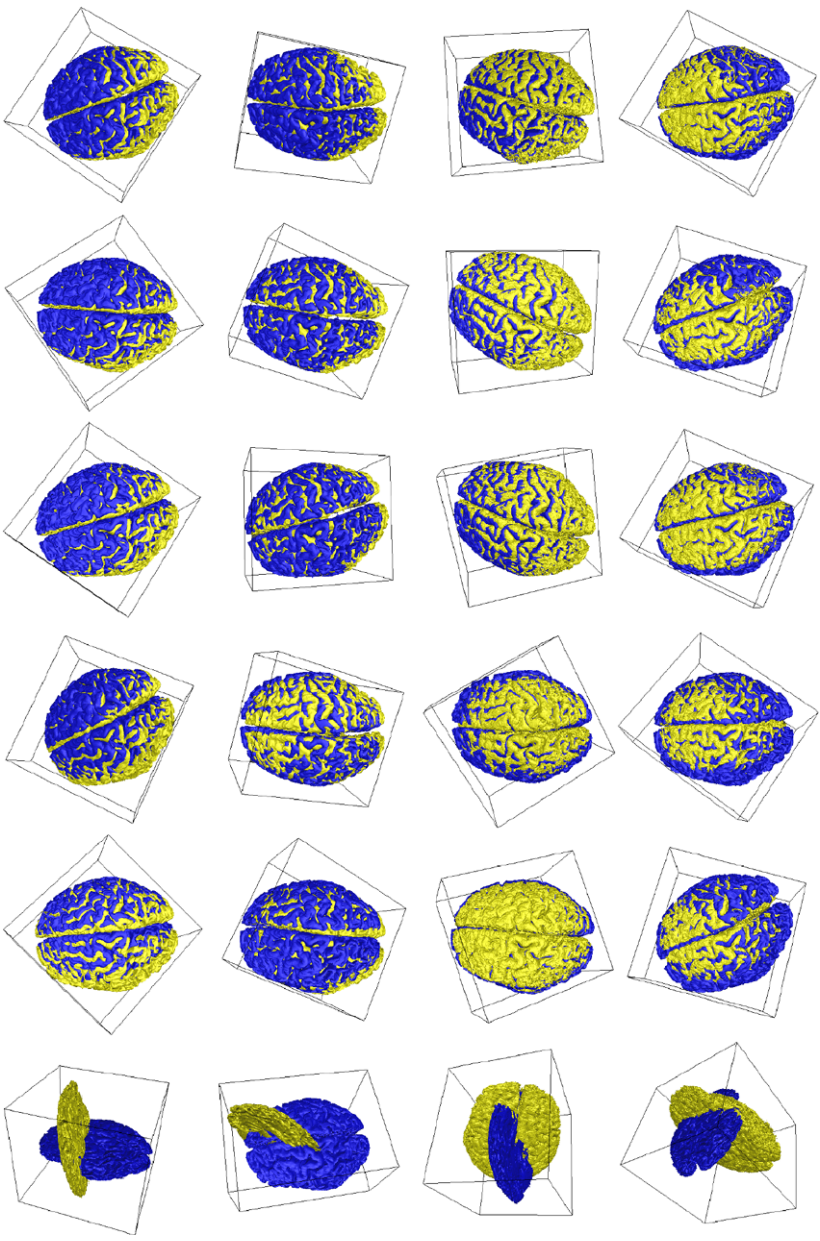

Fig. 9 The *first column* graphically represent the four IR problem instances using MRIs (I_1 vs. $T_1(I_2)$, I_1 vs. $T_2(I_3)$, I_1 vs. $T_3(I_4)$, and I_2 vs. $T_4(I_4)$). *From left to right*, the next columns show the best IR results achieved by GRASP, Stc-G&PR, Dyn-G&PR, Evo-G&PR, and SS IR methods facing each IR problem, respectively

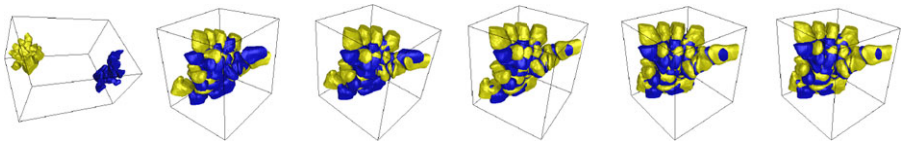

Fig. 10 The *first column* graphically represent the IR problem instance using CT images (I_6 vs. $T_1(I_5)$). *From left to right*, the next columns show the best IR results achieved by GRASP, Stc-G&PR, Dyn-G&PR, Evo-G&PR, and SS IR methods, respectively

Next, we studied the performance of these new IR methods in both realistic and real-world medical applications, using different image modalities such as MRIs and CT images of human brains and human wrists, respectively. We proved how the synergy between the single and multiple trajectory approaches and the evolutionary scheme of PR provided effective and robust results which were competitive with the state-of-the-art point matching-based IR methods based on the SS algorithm. A good trade-off between search space diversification and intensification has achieved the high performance of the new hybrid designs.

Moreover, we compared the tested algorithms with other state-of-the-art IR methods, including the transformation parameters (Dyn-GA), the point-matching (ILS), and a cooperative scheme (ICP+SA) of the latter two approaches. Thus we demonstrated how the combinatorial optimization approach used by the two best algorithms, SS and Evo-G&PR, is an outstanding alternative for tackling IR problem instances of 3D medical images.

In future works, we shall consider the use of new hybrid designs based on GRASP and PR and similar approaches (Lozano and García-Martínez 2010) for tackling the point matching-based IR problem in order to obtain more accurate and robust methods.

Acknowledgements We want to acknowledge Professor J.J. Crisco for providing us the CT images of human wrists. This work was partially supported by the Spain's Ministerio de Ciencia e Innovación (Ref. TIN2009-07727 and TIN2009-07516) and by the Andalusia's Dpto. de Innovación, Ciencia y Empresa (Ref. TIC1619), both including EDRF fundings.

References

Andrade, D.V., Resende, M.G.C.: Grasp with evolutionary path-relinking. In: 7th Metaheuristics International Conference (MIC 2007) (2007)

Arun, K.S., Huang, T.S., Blostein, S.D.: Least-squares fitting of two 3-D points sets. IEEE Trans. Pattern Anal. Mach. Intell. **9**(5), 698–700 (1987)

Brown, L.G.: A survey of image registration techniques. ACM Comput. Surv. **24**(4), 325–376 (1992)

Chow, C.K., Tsui, H.T., Lee, T.: Surface registration using a dynamic genetic algorithm. Pattern Recognit. **37**, 105–117 (2004)

Cordón, O., Damas, S.: Image registration with iterated local search. J. Heuristics **12**, 73–94 (2006)

Cordón, O., Damas, S., Santamaría, J.: Feature-based image registration by means of the CHC evolutionary algorithm. Image Vis. Comput. **22**, 525–533 (2006)

Cordón, O., Damas, S., Santamaría, J., Martí, R.: Scatter search for the 3D point matching problem in image registration. INFORMS J. Comput. **20**, 55–68 (2008)

Dasgupta, S., Banerjee, A.: Pattern tracking and 3-D motion reconstruction of a rigid body from a 2-D image sequence. IEEE Trans. Syst. Man Cybern. **35**(1), 116–125 (2005)

de Falco, I., Della Cioppa, A., Maisto, D., Tarantino, E.: Differential evolution as a viable tool for satellite image registration. Appl. Soft Comput. **8**(4), 1453–1462 (2008)
Faria, H., Binato, S., Resende, M.G.C., Falcao, D.J.: Transmission network design by a greedy randomized adaptive path relinking approach. IEEE Trans. Power Syst. **20**, 43–49 (2005)
Feo, T.A., Resende, M.G.C.: A probabilistic heuristic for a computationally difficult set covering problem. Oper. Res. Lett. **8**, 67–71 (1989)
Glover, F., Laguna, M.: Tabu Search. Kluwer Academic, Dordrecht (1997)
Goshtasby, A.: 2D and 3D Image Registration. Wiley Interscience, New York (2005)
Horn, B.K.P.: Closed-form solution of absolute orientation using unit quaternions. J. Opt. Soc. Am. **4**, 629–642 (1987)
Kim, J., Byun, S., Ahn, B.: Fast full search motion estimation algorithm using various matching scans in video coding. IEEE Trans. Syst. Man Cybern. **31**(4), 540–548 (2001)
Kwan, R.K.S., Evans, A.C., Pike, G.B.: MRI simulation-based evaluation of image-processing and classification methods. IEEE Trans. Med. Imaging **18**(11), 1085–1097 (1999)
Laguna, M., Martí, R.: GRASP and path relinking for 2-layer straight line crossing minimization. INFORMS J. Comput. **11**(1), 44–52 (1999)
Liu, Y.: Improving ICP with easy implementation for free form surface matching. Pattern Recognit. **37**(2), 211–226 (2004)
Lozano, M., García-Martínez, C.: Hybrid metaheuristics with evolutionary algorithms specializing in intensification and diversification: overview and progress report. Comput. Oper. Res. **37**(3), 481–497 (2010)
Luck, J.P., Little, C.Q., Hoff, W.: Registration of range data using a hybrid simulated annealing and iterative closest point algorithm. In: IEEE International Conference on Robotics and Automation (ICRA'00), pp. 3739–3744 (2000)
Marai, G.E., Laidlaw, D.H., Crisco, J.J.: Super-resolution registration using tissue-classified distance fields. IEEE Trans. Med. Imaging **25**(2), 177–187 (2006)
Monga, O., Benayoun, S., Faugeras, O.: From partial derivatives of 3-D density images to ridges lines. In: Computer Vision and Pattern Recognition, IEEE, Champaign, Illinois, USA, pp. 354–389 (1992)
Prais, M., Ribeiro, C.: Reactive GRASP: An application to a matrix decomposition problem in TDMA traffic assignment. INFORMS J. Comput. **12**(3), 164–176 (2000)
Resende, M.G.C., Ribeiro, C.C.: Greedy randomized adaptive search procedures. In: Glover, F., Kochenberger, G. (eds.) Handbook of Metaheuristics, pp. 219–249. Kluwer Academic, Dordrecht (2003)
Resende, M.G.C., Werneck, R.F.: A hybrid heuristic for the p-median problem. J. Heuristics **10**, 59–88 (2004)
Resende, M.G.C., Martí, R., Gallego, M., Duarte, A.: Grasp and path relinking for the max-min diversity problem. Comput. Oper. Res. **37**, 498–508 (2010)
Robertson, C., Fisher, R.B.: Parallel evolutionary registration of range data. Comput. Vis. Image Underst. **87**, 39–50 (2002)
Silva, L., Bellon, O.R.P., Boyer, K.L.: Precision range image registration using a robust surface interpenetration measure and enhanced genetic algorithms. IEEE Trans. Pattern Anal. Mach. Intell. **27**(5), 762–776 (2005)
Wachowiak, M.P., Smolikova, R., Zheng, Y., Zurada, J.M., El-Maghraby, A.S.: An approach to multimodal biomedical image registration utilizing particle swarm optimization. IEEE Trans. Evol. Comput. **8**(3), 289–301 (2004)
Wang, F.: An efficient coordinate frame calibration method for 3-D measurement by multiple camera systems. IEEE Trans. Syst. Man Cybern. **35**(3), 453–464 (2005)
Yamany, S.M., Ahmed, M.N., Farag, A.A.: A new genetic-based technique for matching 3D curves and surfaces. Pattern Recognit. **32**, 1817–1820 (1999)
Zitová, B., Flusser, J.: Image registration methods: a survey. Image Vis. Comput. **21**, 977–1000 (2003)